North-Gondwana – Laurussia dynamic paleogeography challenged by magnetic susceptibility through the Famennian

Catherine Girard, Raimund Feist, Angelo Mossoni, Jean-Jacques Cornee,
Pierre Camps, Anne-Lise Charruault, Carlo Corradini

Highlights

Early Famennian MS values differ on N-Gondwana and on S-Laurussia margins

Famennian MS values correlate with conodont biofacies

MS is a powerful tool for geodynamics
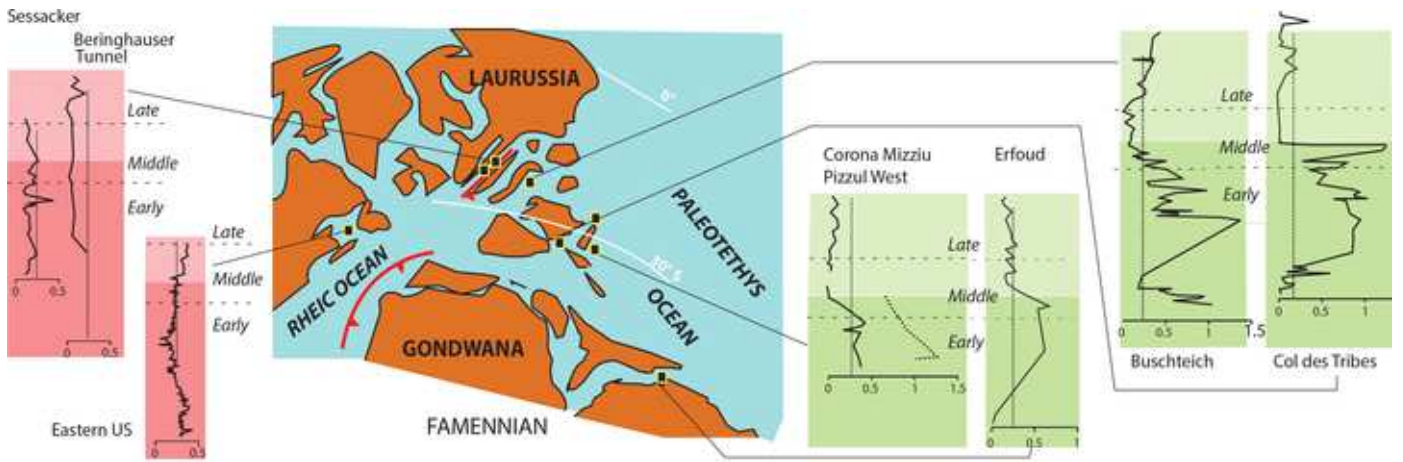
Highlights

Early Famennian MS values differ on N-Gondwana and on S-Laurussia margins

Famennian MS values correlate with conodont biofacies

MS is a powerful tool for geodynamics

Graphical Abstract

North-Gondwana - Laurussia dynamic paleogeography challenged by

magnetic susceptibility through the Famennian

Girard, Catherine[1*]; Feist, Raimund[1]; Mossoni, Angelo[2]; Cornée, Jean-Jacques[3];

Camps, Pierre[3]; Charruault, Anne-Lise[1]; Corradini, Carlo[4]

[1]*Institut des Sciences de l'Evolution de Montpellier (ISEM), Univ Montpellier, CNRS, EPHE,*

IRD, Montpellier, France.

[2] *2 Kingsdown court, 56 Bolingbroke grove, London SW11 6HS, UK*

[3] *Géosciences Montpellier, Université de Montpellier, CNRS, and Université des Antilles,*

Montpellier and Pointe à Pitre, (FWI), France

[4] *Università degli Studi di Trieste, Dipartimento di Matematica e Geoscienze, Trieste, Italy*

*corresponding author (catherine.girard@umontpellier.fr)

18

19 **Abstract**

20 Large-scale magnetic susceptibility (MS) variations in ancient sediments are usually

21 interpreted as related to sea-level and climate changes affecting the erosional regime and the

22 amount of detrital input. To constrain such environmental changes during the Famennian, we

23 compared MS records in representative sections of pelagic limestones of (1) the Avalonian

24 margin of Laurussia [Sessacker (SES) and Beringhauser Tunnel (BHT), Rhenish Slate

25 Mountains, Germany] and (2) in Gondwana related terranes [Erfoud (ERF), Tafilalt,

26 Morocco; Col des Tribes (CT), Montagne Noire, France; Buschteich (BU), Thuringia,

27 Germany; Corona Mizziu (CM I, II), Sardinia and Pizzul West (PZW) in the Carnic Alps,

28 Italy]. Very low MS values throughout the Famennian characterize sections from Avalonia. In

29 contrast, MS values are high and oscillating in Gondwana during the early Famennian; they

30 drop significantly all together in the middle Famennian *Palmatolepis marginifera marginifera*

31 Zone to match the pattern of low MS values of the Avalonian margin thereafter. To evaluate

32 the importance of partial diagenetic overprint, MS data were compared to hysteresis

33 parameters and geochemical proxies in sections BU, CM I, II and CT. The degree of thermal

34 diagenesis is estimates taking into account the Color Alteration Indices (CAI) of conodonts.

35 Striking dissimilarities in MS records between Laurussia and Gondwana are in favor for an

36 existing remnant oceanic barrier between these continents during early Famennian times,

37 when the amount of detrital supplies was obviously different. Uniformity is reached after the

38 drop of MS values in N-Gondwana, when oceanic barriers could have vanished during the

39 early middle Famennian T-R fluctuations of the sea-level. All sites remained under a rather

40 similar regime of detrital supply through middle to uppermost Famennian. Comparison of MS

41 trends with trends of conodont biofacies in five sections (CT, BU, CM I, II and SES) allows

42 emphasizing the concordance of their relationship to sea level fluctuations.

1
2
3
4
5
6
7
8
9
10
11
12
13
14
15
16
17
18
19
20
21
22
23
24
25
26
27
28
29
30
31
32
33
34
35
36
37
38
39
40
41
42
43
44
45
46
47
48
49
50
51
52
53
54
55
56
57
58
59
60
61
62
63
64
65

1. Introduction

Low-field magnetic susceptibility (MS) is currently considered a proxy to assess the amount of detrital inputs in relation to sea level changes, integrating mineralogical and sedimentological information on their nature and origin (e.g. Ellwood et al. 2006, 2007, 2008, Hladil 2002, Da Silva et al. 2009, 2010). As such it may constitute a powerful and independent proxy to control global trends of sea level changes on condition that the primary origin of low-field magnetic susceptibility is demonstrated. This can be done by comparing MS values with hysteresis parameters and/or elemental concentrations (Devleeschouver et al. 2010); Riquier et al. 2010). Color Alteration Indices (CAI) of conodonts are taken into account to estimate the degree of thermal diagenesis of the rock samples (Epstein et al. 1977). Indeed, the coulor of the conodonts is related to the temperature that affected the rocks. With an average MS value for lithified marine deposits of $5.5x10^{-8}$ m^3/kg (Ellwood et al. 2011a) most of Paleozoic limestones range between 0.1 and $10x10^{-8}$ m^3/kg (Ellwood et al. 2006). This is the case in Devonian off-shore carbonate successions where a fair number of MS investigations (e.g. Crick et al. 2002, Da Silva et al. 2009, Ellwood et al. 2011b, Riquier et al. 2010) were conducted since the first global sea-level curve was established by Johnson et al. (1985).

Comprehensive spatio-temporal investigations combining variations of litho- and biofacies with isotope data indicate a long term Famennian regressive trend (Johnson et al. 1985) that is punctuated by short transgressive episodes/events such as at the base of the Famennian (Sandberg et al. 2002). However, within-section MS evolution remains sometimes difficult to correlate with precision between sedimentary sequences from different paleogeographic entities (e.g., Crick et al. 2002). Attention is drawn to the possibility that MS signal in carbonate systems may be affected by diagenesis (Da Silva et al 2012, Devleeschouwer et al.

71 2015), or casually indicate rather particular local conditions (Davies et al. 2013) in spite of

72 global eustasy.

73 Indeed, both the amount and nature of detrital material may possibly be disturbed by aeolian

74 or volcanic inputs, heterogeneity of climatic influence in the continental source areas, and by

75 the importance of physical action during gravitational transport (e.g., current-induced re-

76 working, debris-massflows). On the contrary, slow sedimentation rates or absence of

77 deposition leading to hardgrounds and hiatuses may result in different records of MS signals

78 and their amplitudes. MS studies have been mainly focused on episodes of major extinction

79 events such as the terminal Frasnian Kellwasser events that are particularly marked by

80 instabilities of the sea-level (e.g., Averbuch et al. 2005, Riquier et al. 2010). According to

81 these authors, the increase of detrital input related to the marked sea-level fall in the earliest

82 Famennian post-event period is expressed by a significant increase in the MS signals.

83 Noticeably, the values of this excursion is particularly less marked in sections on the

84 Avalonian margin of Laurussia than in those of the Gondwana margin (Averbuch et al. 2005,

85 fig. 4) (Fig. 1).

86 In this contribution we carry out investigations on the entire Famennian from representative

87 sites of both N-Gondwanan and Avalonian terranes to allow the evaluation of the extent to

88 which the environmental changes of approaching Laurussia/Gondwana margins may have

89 influenced the MS signals (Fig. 1a). To this end, we conducted an integrated study of MS,

90 hysteresis parameters and element concentrations, in some sections (CM I, CM II, PZW and

91 partially in BU), in order to test whether MS can be considered as a reliable detrital proxy.

92 Following Riquier et al. (2010), some elements characteristic of the terrigenous input are not

93 affected by diagenesis (e.g., Zirconium) and can be used as a proxy of the bulk magnetic

94 mineralogical component (Total Fe). Thereafter, we will compare MS measurements with

95 analyses of conodont biofacies in sections that provide sufficient amounts of conodont

5

96 elements. Indeed, conodonts can also characterize palaeo-environments because of the

97 different ecological preferences of the various genera (Sandberg 1976, Seddon and Sweet

98 1971, Girard et al. 2020), indicative of distance regarding the shoreline. According to this

99 view, the changes in the relative proportion of the different genera, namely biofacies, have

100 been proven useful to track environmental changes through time (e.g., Corradini 2003, Girard

101 et al. 2014, 2017, 2020). As a prerequisite, the continuity of MS records is controlled by fine-

102 scaled conodont biostratigraphy of Spalletta et al. (2017), updated in the latest Famennian by

103 Corradini et al. (2021).

104 Whether trends in combined MS and biofacies curves allow constituting characteristic

105 features of Famennian deposits in general, and to what extend they are permanent or are

106 restricted to a definite duration, are prime subjects of our investigations. They allow pointing

107 possible causes that we aim to discuss.

108

2. Famennian sections

110 The investigated sections, CT, BU, PZW, CM, ERF, BHT, SES (and DGHS for comparison)

111 are situated between north Gondwana and Laurussia at tropical to subtropical paleolatitudes

112 (Fig. 1a). The position of some samples, conodont zones and main lithofacies are shown in

113 columnar sections Figure 1b.

114

2.1. North Gondwana sections

116

Col des Tribes (Montagne Noire, France).

118 This section (72 m-thick) was described by Girard et al. (2014). It is composed of (from

119 bottom to top): - bioclastic limestones (17 m- thick) organized into dm- thick beds; - massive,

120 red mudstones to wackestones/floatstones (15 m- thick) organized into dm- thick beds

6

121 yielding abundant cheiloceratid goniatites (Griottes facies); - massive micritic limestones (20

122 m- thick) organized into dm- thick beds; - pseudo-nodular limestones (15 m- thick) composed

123 of cm- thick beds which have experienced pressure-dissolution processes; - massive micritic

124 limestones (5 m- thick). These sediments were deposited in mid ramp to basin settings.

125 Abundance of conodonts allows establishing a fine–scaled biozonation from the *Pa. rhenana*

126 (late Frasnian) to the *Bi. ultimus* Zone (*Pr. meischneri* Subzone, latest Famennian). In this

127 section conodonts are relatively well preserved, with a low Conodont Alteration Index (CAI)

128 ~ 2-2.5 (temperature range = 60 to 110°C).

129

130 **Buschteich (Thuringia, Germany)**.

131 This section (35 m- thick) was studied by Girard et al. (2017). From bottom to top, it is

132 composed of: - cm bedded to pseudonodular wackstones (3 m- thick) (Frasnian); - dm to m-

133 thick beds of mudstones to wackestones (7 m- thick); - mud-wackestones and pseudonodular

134 mudstones (7 m- thick); mm to cm- bedded mud-wackestones (10 m- thick); - mm to cm

135 bedded to pseudonodular wackestones, and some clay (8 m- thick). These sediments were

136 deposited in outer ramp to basin settings. The section spans an interval from the *Pa. rhenana*

137 to *Bi. ultimus* (*Pr. meischneri* Subzone) conodont Zones, but the lowest part of the Famennian

138 is missing (from *Pa. subperlobata* to *Pa. minuta minuta* Zones). The CAI of conodonts is

139 high, estimated as 4 (temperature range = 190 to 300°C).

140

141 **Pizzul West (Carnic Alps, Italia)**.

142 This section (24 m- thick) was described by Mossoni et al. (2014), and Corradini et al. (2017).

143 From bottom to top, it comprises: - massive to nodular grey mudstones to packstones (16.5 m-

144 thick); - red nodular wackestones to packstones (7.5 m- thick) (Griottes facies). The

145 limestones contain few fossils. The Griottes facies comprises nodules up to 1 cm of diameter

146 coated with hematite precipitations probably due to synsedimentary diagenesis. The

147 sediments were deposited in mid to outer ramp settings. The section spans an interval from

148 the *Pa. glabra prima* to *Pa. marg. marginifera* Zones. The CAI of conodonts is around 4

149 (temperature range = 190 to 300°C).

150

Corona Mizziu I and Corona Mizziu II (Sardinia, Italia).

151

152 The Corona Mizzu sections have been studied by Corradini (1998, 2003).

153 The Corona Mizziu I (CM I) section (30 m- thick) comprises beds of poorly fossiliferous

154 mudstones, with wackestone to packstone beds in the middle part of the succession.

155 Sediments were deposited in a pelagic setting. The conodont data allow discriminating twelve

156 conodonts zones from the *Pa. rhomboidea* Zone up to the *Bi. ultimus* Zone.

157 The Corona Mizziu II (CM II) section (18 m-thick) crops out a hundred meters apart from the

158 CM I section and exposes grey massive monotonous mudstones with poor fossil remains. The

159 tectonic imprint is marked by stylolite structures and calcite recrystallization. Sediments were

160 deposited in a pelagic setting. The section spans a time from the *Pa. crepida* to the *Pa. rugosa*

161 *trachytera* Zones. For these two sections (CM I and CM II), the CAI of conodonts is very

162 high, with values near 4.5 – 5 (temperature range = 300 to 400°C).

163

Erfoud (Tafilalt, SE Morocco).

164

165 The Erfoud section spanning the entire Late Devonian has been described by Buggisch &

166 Clausen (1972). The considered lower to middle Famennian part of the section (8 m- thick)

167 was re-sampled. It comprises from bottom to top: - 3 m-thick dark grey mud to wackestones

168 and black shales, with dm-thick beds with cephalopods and bivalve remains (Kellwasser

169 Limestone facies); - 0.45 m- thick platy red-brownish and grey-olive microsparitic calcilutites

170 with bioclasts and Fe-oxid coated oncoids ; - 1.10 m-thick grey-brown cephalopod calcilutites

8

171 with Fe-oxid coated intraclasts; - 1.95 m-thick thin-bedded nodular calcilutites with

172 cephalopods and trilobites ; -1.50 m- thick alternating cm- thick bedded beige argillaceous

173 nodular limestones and marls. In the lower part of the section the *Pa. crepida* Zone is

174 extremely condensed at the top of the dysoxic black Kellwasser-type limestone. The latter

175 characterises a dysoxic bottom sea depositional environment. Above the Kellwasser

176 limestones, the depositonal conditions reflect low sedimentation rates in an open outer shelf

177 environment within the photic zone as testified by prevaling large-eyed trilobites (deep inner

178 to mid ramp). The section encompasses the interval of the *Pa. subperlobata* to the *Pa. rugosa*

179 *trachytera* Zones with a gap between the *Pa. termini* to *Pa. gracilis gracilis* Zones (Fig. 1b).

180 Conodonts have a CAI of 3-4 (temperature range = 150 to 300°C).

181

182 *2.2. South Laurussia sections*

183

184 **Beringhauser Tunnel (Rhenish Slate Mountains)**.

185 This section (15 m- thick) was studied by Schülke & Popp (2005). It consists of mainly well-

186 bedded massive to subordinately nodular cephalopod limestones. At the top of the section,

187 facies change from massive limestones to nodular limestones. Sediments were deposited in

188 mid to outer ramp setting. The considered section spans a time from the *Pa. crepida* to the *Pa.*

189 *rugosa trachytera* Zones. The CAI of conodonts is high, about 4.5 (Joachimski et al. 2009),

190 (temperature range around 300°C).

191

192 **Sessacker (Rhenish Slate Mountains)**

193 This highly condensed section (2.5 m- thick) was studied by Ziegler (1962) and Schülke

194 (1999), and complemented by new data. It consists of red mudstones to wackestones with

195 cephalopods, and some sparitic intercalations occur. The sediments were deposited in outer

9

196 ramp setting. The section spans from the *Pa. delicatula platys* to the *Pa. rugosa trachytera*

197 Zones. The conodonts are well-preserved with a CAI around 2.5 (temperature range = 60 to

198 110°C).

199

200 **Dupont GHS drillhole (Illinois basin, Eastern North America).**

201 Drillcores in the Chattanooga Shale of Illinois revealed fine-grained siliciclastic sediments (9

202 m- thick) dating Famennian (Over et al. 2019). Conodont assemblages indicate that the

203 section spans the *Pa. glabra prima* to *Bi. ac. aculeatus* Zones. MS values are low, in the -

204 0.25/-0.75 interval.

205

206 **3. Methods**

207

208 *3.1. Magnetic Susceptibility*

209 The samples studied are from previous collections for CT (Girard et al. 2014), BU (Girard et

210 al. 2017), CMI and II (Mossoni 2014), PZW (Mossoni 2014). 129 new samples from sections

211 SES, BHT and ERF have been analysed. We measured the low field magnetic susceptibility

212 (χLF), abbreviates as magnetic susceptibility (MS) for the seven representatively distributed

213 Famennian sections.

214 At Col des Tribes (CT, Montagne Noire, France) the field magnetic susceptibility (MS) was

215 directly measured in situ with the Bartington MS2E sensor connected to the MS3 meter. To

216 ensure a representative result, five measures were performed and then averaged for the 74

217 successive stratigraphic levels (Supplementary Data, Table S1). Ex-situ measurements were

218 performed in the laboratory on block samples from German (63 samples for BU, 26 for SES,

219 and 15 BHT) and Moroccan (25 samples for ERF) sections with the same device and the same

220 protocol involving a minimum of 2 measurements per level (Supplementary Data, Tables S2,

10

221 S3, S4 and S5). Samples from the italian sections (Pizzul West and Corona Mizziu I, II were

222 measured with the KLY-3S Kappabridge at the University of Liège (Supplementary Data,

223 Tables S6, S7, S8).

224 All the MS data figured represent an average of the measurements (Fig. 2) expressed in 10^{-8}

225 m^3/kg for readability. Following the age model published by Girard et al. (2020), the base of

226 conodont zones was dated by means of absolute age estimates provided by Becker et al.

227 (2012), and updated by Becker et al. (2020), and all MS data were figured based on the

228 estimated absolute ages (Fig. 2).

229

230 *3.2. Hysteresis parameters*

231

232 The Italian sections (CM I, CM II and PZW) were prepared for hysteresis loops (Mossoni

233 2014) with the objective to roughly estimate the nature of the ferromagnetic (*sensu lato*) Fe-

234 oxides. Indeed, as red nodular facies occur in Pizzul West but not in Corona Mizziu sections,

235 we have suspected significant differences in the nature, the oxidation state, and the

236 concentration quantity of strongly oxidized Fe-oxides such as hematite in the former section,

237 and non-oxidized Fe-oxides such as magnetite in the later section. The hysteresis loops were

238 measured with the J-Coercivity "rotation" magnetometer at Dourbes IRM Geophysical

239 Centre, respectively (Supplementary Data, Tables S8, S9, S10).

240 For the hysteresis measurements, the specimens were prepared from blocks taken every 10

241 cm all along the studied cross-sections. We calculated from the hysteresis loops the high-field

242 magnetic susceptibility (χHF) and the ferromagnetic susceptibility (χferro) following methods

243 developed in Riquier et al. (2010), and Da Silva et al. (2012, 2015). These two parameters

244 allow assessing the respective contribution of the para/dia-magnetic minerals (χHF) and the

245 ferromagnetic minerals to the initial susceptibility. At the end of the hysteresis loop

11

246   acquisition, the magnetic viscosity coefficient was calculated from the remanence decay,

247   which was monitored for 100s after the field was removed.

248   Additionally, the major elements (Al, Si, K and Ti) were considered to estimate the

249   proportion of minerals in terms of their magnetic amounts for17 samples in PZW, 13 samples

250   in CM I and 14 samples in CM II (Tables PZW, CM I and CMII). These analyses on major

251   elements were performed with an X-Ray Fluorescence (Panalytical MagiX PW2540) device

252   at the University of Cagliari. The powder disks were prepared using at least 20 grams of

253   the sample mixed with polyvinyl alcohol, on a base of boric acid. The total amount of oxides

254   and LOI (loss on ignition) has been considered acceptable for samples with an error of ±2%.

255   In order to have comparable results between the studied sections, all analyses were

256   normalized to 100. In this way a small error percentage has been distributed between all the

257   measured parameters (Supplementary Data, Tables S8, S9, S10).

258

259   *3.3. Detrital vs authigenic Fe content*

260   To further constrain the diagenetic versus detrital imprints on MS, we compared the low-field

261   magnetic susceptibility (χHF) variations with selected geochemical proxies measured by

262   mean of the methods developed by Riquier et al. (2010). X-Ray Fluorescence analyses were

263   performed on the samples of Buschteich which presents no signs of strong oxydation and is

264   the most complete section of this study. The analyses were performed with the Niton XL3t-

265   900 Goldd X-ray fluorescence portable analyzer (Thermo Scientific®, Waltham, MA, USA)

266   at the University of Montpellier. All the rock samples were carefully cleaned prior to all

267   treatment, and weathered surfaces were removed.

268   We selected elements that can be used as proxies for the terrigenous input. The Zirconium

269   (Zr) was selected here as the more reliable detrital proxy because it is not affected by

270   diagenesis; and the total Fe (Fe_{tot}) content will be used as a proxy of the bulk magnetic

12

271 mineralogical component. The total Fe was separated into an inherited detrital part and a

272 secondary authigenic part. Following Riquier et al. (2010), the detrital and authigenic

273 fractions of the total iron content were estimated considering that the Fe/Al ratio of the

274 detrital part of the studied rocks is supposed to be the same as that of the average shale value

275 (Fe/Al$_{average\ carbonate}$; 0.55 Clarkson et al. 2014). The detrital fraction of iron (Fe$_{det}$) is

276 calculated as Fe$_{det}$ = Al$_{sample}$ * Fe/Al$_{average\ carbonate}$. Consequently, the iron fraction in excess

277 relative to the detrital fraction, namely, Fe$_{exc}$ = Fe$_{tot}$ - Fe$_{det}$, may be considered to be of

278 authigenic/diagenetic origin.

279

3.4. Biofacies

281 Five sections were sampled in detail for conodont biofacies based on conodont genera

282 abundances. Conodont biofacies are advocated to be mostly driven by water depth variations

283 due to the habitat preferences of the different conodont genera (e.g., Sandberg 1976, Seddon

284 and Sweet 1971). In this regard, the distribution of conodont genera is thought to be

285 controlled by water depth along a proximal-distal gradient (Klapper and Barrick 1978, Girard

286 et al. 2020), and as such may constitute a proxy of sea-level variations and indirectly of

287 detrital input. Several biofacies can be defined, based on the percentage of different genera

288 present in the samples from biofacies characterized by distal surface dwellers (*Palmatolepis*)

289 to proximal surface dwellers (*Icriodus*). The percentages of conodont elements per genus,

290 later on called biofacies, were estimated for samples of each section: 74 samples for CT

291 (Girard et al. 2014), 34 samples for BU (Girard et al. 2017), 12 samples for SES (Schülke

292 1995; this study), 13 samples in CM I and 13 samples for CM II (Corradini 2003, Mossoni

293 2014). All data are available in the Supplementary Data, Table S11. As MS is also known to

294 be related to detrital input, we compared the MS trends of these five sections with trends in

295 percentage of conodont genera (biofacies). A Principal Component Analysis (PCA on the

13

296 variance - covariance matrix) allows summarizing biofacies of the five considered sections

297 (CT, BU, CM I and CM II, and SES) on few synthetic axes. This analysis also provides a

298 representation of the records of CT, BU, CM I, CM II and SES on the same synthetic axes,

299 allowing a direct comparison of the biofacies variations in the five outcrops. The contribution

300 of each genus percentage to the axes allowed their interpretation in relation to the biofacies.

301 Correlations between the MS and PC values are calculated using Pearson's product-moment

302 correlation to investigate if MS and PC values are correlated or not.

303

4. Results

4.1. Magnetic susceptibility data

306 The relationship between the absolute age of the base of the biozone boundaries and

307 sediment thickness allows establishing an age model for each section. The ages estimated for

308 each sample were thereafter used to plot the variations of magnetic susceptibility through

309 time. When we compare the evolution of magnetic susceptibility (MS) of Famennian

310 sequences in the different sections, various types of record are documented (Fig. 2):

311 - In the investigated sections of the North Gondwana shelf (Morocco, Montagne Noire), MS

312 values vary markedly and congruently during early Famennian times: initially high and

313 fluctuating MS values shift all together to low ones within the *Pa. marginifera marginifera*

314 Zone (initial mid-Famennian), and remain constantly low thereafter, lower than the common

315 Paleozoic magnetic susceptibility values (around 5.5×10^{-8} m^3/kg).

316 - In the most distal sections of the Gondwana shelf (Sardinia, Carnic Alps, Thuringia), the

317 same trend is observed but fluctuations are less pronounced during the lower Famennian with

318 temporary increases in MS values before the *Pa. marginifera marginifera* Zone.

14

319 - In south Laurussia (DGHS section), the MS values remain low throughout the record, almost

320 always less than the average of 5.5×10^{-8} m^3/kg, being rather close to the common Paleozoic

321 magnetic susceptibility values.

322 - In the Avalonian outer shelf areas of Laurussia (SES and BHT), the MS values are very low

323 during the early Famennian and are similar to those of both Laurentian (DGHS, Fig. 1) and

324 north Gondwanan terranes during mid-through late Famennian times.

325 In summary, in the north Gondwana margin a two-fold stage subdivision of the magnetic

326 susceptibility curve is observed. During the lower Famennian, increasing high values are first

327 recorded then followed by decreasing values that culminate during the *Pa. marginifera*

328 *marginifera* Zone. During the middle to upper Famennian, MS values remain lower than the

329 common Paleozoic magnetic susceptibility values (vertical dotted line in Figure 2). The major

330 shift from high to low MS values during the *Pa. marginifera marginifera* Zone in Gondwana

331 is not recorded in the Laurussia section where MS values remain low through the entire

332 Famennian.

333

4.2. Magnetic hysteresis data

335 For the Italian sections PZW, CM I and CM II, the correlations of oxides representing

336 terrigenous input with the MS data are shown in the Supplementary Data (Fig. S1), and

337 detailed in Table 1.

338 For the Pizzul West section, a significant correlation exists between the low field magnetic

339 susceptibility (χ_{LF}) and ferromagnetic contribution (χ_{ferro}), but not with the high field magnetic

340 susceptibility (χ_{HF}). A correlation between low field magnetic susceptibility (χ_{LF}) and the

341 geochemical parameters is not observed (Al_2O_3=0.005, SiO_2=0.12, TiO_2=0.12, K_2O=0.04)

342 (Table 1). However, there is a highly significant correlation between the high field magnetic

343 susceptibility (χ_{HF}) and geochemistry (Al_2O_3=0.84, SiO_2=0.81, TiO_2=0.85, K_2O=0.83), that

344 demonstrates that the paramagnetic fraction is linked to Al, Si, K and Ti bearing minerals.

345 As most of the Hcr values are lower than 60mT, the MS variations are probably related to low

346 coercivity minerals as magnetite.

347 For the CM I section a strong correlation exists between the low field magnetic susceptibility

348 (χ_{LF}) and the high field magnetic susceptibility (χ_{HF}), and the ferromagnetic contribution

349 (χ_{ferro}). This demonstrates that the paramagnetic fraction is linked to Al, Si, K and Ti bearing

350 minerals. A very good correlation also exists between the low field magnetic susceptibility

351 and the four measured oxides (Al_2O_3=0.68, TiO_2=0.70, K_2O=0.69) (Table 1).

352 For the Corona Mizziu section II, the low field magnetic susceptibility has a good correlation

353 with χ_{ferro} (r = 0.85) and with χ_{HF} (r = 0.82) (Table1). This suggests that the low field magnetic

354 susceptibility of the Corona Mizziu II section is controlled by both the ferromagnetic and

355 paramagnetic contributions. All the MS values are extremely low (lower than 3.0×10^{-8}

356 m^3/kg, indicating the influence of the diamagnetic fraction, which may have diluted the

357 potential detrital signal.

358 The magnetic signal for Pizzul West section would be mainly controlled by ferromagnetic

359 contribution of low coercivity mineral (likely magnetite), whereas, for the Corona Mizziu I

360 and II sections, the magnetic signal seems to be influenced by dia and/or paramagnetic

361 contributions and, to a lesser extent, by ferromagnetic contribution.

362

4.3. MS correlation to Fe content

363

364 Both measured Fe_{tot} and calculated Fe_{det} correlate with the MS evolution (r = 0.46, p = 0.002

365 for Fe_{det} and r = 0.41; p = 0.0005 for total Fe). The Fe_{exc} does not show a correlation with the

366 MS variations (r = 0.19, p = 0,157). A correlation exists between MS and the Zr content

367 (r=0.28, p = 0.037) as well as between the MS and the Fe/Zr ratio (r=0.73, p<0,001).

16

368 (Supplementary Data, Fig. S2 and Supplementary Data, Table S2). Although this theoretical

369 calculation gives an estimate of the Fe-bearing fractions only, Fe_{det} and Fe_{exc}, it supports the

370 coexistence of a detrital component, controlling the MS evolution in Buschteich, and an

371 authigenic component, that could have induced the widespread remagnetization process

372 observed in these carbonates. This means that for the Buschteich section we cannot exclude

373 that a part of the signal results from diagenetic processes, but this part is not as significant as

374 the detrital part.

375 In summary, the geochemical data show that, although in part affected by diagenesis, as

376 shown by correlation between MS and Fe/Zr, MS can be used as an indicator of the detrital

377 input evolution in the studied Famennian sections. It is consequently possible to use it as a

378 proxy of sea level variations which can be compared to the conodont biofacies proxy.

379

4.4. Comparison with conodont biofacies

381 The principal component analysis performed on the proportions of different genera allows

382 summarizing the biofacies variations (Fig. 3) on main axes that express the total variance. The

383 record of the five sections CT, BU, CM I, CM II (North Gondwana) and SES (South

384 Laurussia) can be directly compared on these axes.

385 The first axis (PC1, 75.8% of the total variance) of the principal component analysis on

386 conodont percentages shows a progressive trend to positive values (from 0 to 1) through the

387 early Famennian. This trend reverses in the early mid – Famennian to negative values (Fig.

388 3b). The contribution of the variables (here, the percentages of the different genera) to the

389 axes (Fig. 3b) shows that positive values along the first axis correspond to a high proportion

390 of *Palmatolepis* whereas negative values correspond to a high proportion of *Bispathodus*

391 (Supplementary Data, Table S11). A correlation (N = 115; r = 0.26; p < 0.005) exists between

392 the PC1 and the MS data. The third axis represents only < 4% of variance, and mostly

17

393 corresponds to variations in the proportion of *Icriodus* in the early Famennian : peaks from

394 *Pa. triangularis* to *Pa. crepida* Zones in CT, peak in the *Pa. crepida* Zone in BU, peak from

395 the *Pa. glabra prima* to the *Pa. rhomboidea* Zones for CM, peak from *Pa. delicatula platys* to

396 *Pa. minuta minuta* in SES (Supplementary Data, Table S1, and Fig. 3c), but values on the

397 PC3 axis are not correlated with the MS values.

398

5. Discussion

400 Since pelagic carbonates are dominantly microsparites of diagenetic origin (Franke &

401 Walliser 1983), one can only speculate on the ultimate source of the MS signals as these may

402 be variously impacted by post-depositional processes. Following intervening aspects are

403 discussed:

404

5.1. Impact of diagenesis

406 The magnetic susceptibility of a rock depends on both the mineralogical composition

407 of the rock and the proportion of each mineral. The three main magnetic behaviours are:

408 diamagnetic minerals (such as carbonates and quartz) displaying extremely weak negative MS

409 values; paramagnetic minerals (e.g., clay minerals, particularly chlorite, smectite, illite and

410 glauconite, ferromagnesian silicates, iron and manganese carbonates, pyrite) displaying weak

411 positive values, and ferromagnetic minerals (mainly magnetite, pyrrhotite, maghemite, and

412 hematite) displaying strong positive values (Da Silva et al. 2010). Diagenetic and post-

413 diagenetic processes lead to mineralogical and chemical transformation of iron oxides that in

414 turn influences the MS values. Riquier et al (2010) showed that although submitted to

415 different burial histories and diagenetic conditions, consistent long-term trends can be

416 observed in the MS evolution from sections through the Frasnian-Famennian boundary. Their

417 data demonstrated that the MS evolution of the carbonate sections they studied can be

18

418 interpreted in terms of paleoenvironmental changes along the former margins of Laurussia

419 and Gondwana.

420 In Pizzul West and Corona Mizziu, the conodont Color Alteration Index (CAI) ranges

421 between 4.5 – 5.5. The temperature (200-400°C) which affected the rocks is far beyond the

422 temperature of the goethite-hematite transition. Thus, the high coercivity values measured are

423 related to the presence of hematite, visible also in the microfacies (Mossoni 2014). However,

424 where high coercivity minerals control the MS (χLF), the presence of hematite is here

425 interpreted to be of detrital origin because both the high field magnetic susceptibility (χHF)

426 and the viscous decay do not correlate.

427 At Buschteich, the Fe in excess does not modify the general trend of MS, at least not

428 enough to overprint the detrital signal.

429 In the CT section, CAI values of 2 – 2.5 were measured by Wiederer et al (2002), that

430 corresponds to burial temperature of less than 100°C. Low illite crystallinity indicates that the

431 site underwent anchizonal metamorphism at maximum. We assume therefore that a part of the

432 MS signal, associated to iron-bearing primary clay minerals, has been preserved in the N-

433 Gondwana sections despite different diagenetic stories.

434 Trends in MS are similar on the N-Gondwana margin (CAI estimed to 4-5 in PZW,

435 CMI and II, BU and around 2-2.5 for CT), high values during the early Famennian and low

436 values during mid-late Famennian. Similar patterns also occur in the S-Laurussia margin

437 (CAI near 4 for BHT and only 2-2.5 for SES), but values remain low during the Famennian.

438 This indicates that, despite different burial histories, the primary MS signature was not

439 overprinted by the diagenetic signal, and it reflects in part its detrital origin.

440

441 *5.2. Relations between depositional setting and MS*

442   Variations in the amount of detrital ferromagnetic minerals in off-shore cephalopod

443   limestones may be of different origins, and, in consequence, it is often difficult to precisely

444   determine the cause of changing MS values and their amplitudes (e.g. Devleeschouver et al.

445   2015). In this regard, the depositional conditions of the investigated sections could play a role

446   on the accumulation of ferromagnetic minerals.

447   In the Rhenish Slate Mountains (SES, BHT), the Upper Devonian cephalopod

448   limestones were deposited upon deep submarine rises beyond direct influence of sea-level

449   changes (Franke & Walliser 1983). Besides *in situ* precipitation, pelagic carbonate mud

450   originated from shallow-water areas. Fine-grained sand and clay fractions, originated from

451   distal turbidites deposition, have also probably reached the rises but they mostly have been

452   winnowed away by bottom currents. Consequently, rather low MS values might reflect

453   presence low amount of transported ferro-magnetic elements, as coarse detrital influxes from

454   northern shelf margins were concentrated in sandstone turbidite bodies that by-passed and

455   were dispatched in troughs between the rises.

456   In the Montagne Noire (CT), very high MS values are recorded during the *Pa. marginifera*

457   *marginifera* Zone prior to a sudden shift to low values under more stable environmental

458   conditions in deeper mid-Famennian outer ramp setting. This shift is coincident with an

459   abrupt change in facies: high though strongly oscillating values are found in the famous red-

460   colored Griottes facies (Tucker 1974) and low values in the overlying compact light grey

461   carbonate mudstones. The Griottes facies is a cephalopod-rich, nodular limestone with

462   abundant iron-clay coatings and some ferruginous hard-grounds. The MS values in this facies

463   are influenced by different chemical and/or physical constraints, not only the detrital inputs of

464   ferro-magnetic minerals. Indeed, ferrugineous mineral phases accumulations may also be

465   influenced by changing both bottom sea oxygenation and rates of Fe-oxide –reduction related

466   to buried organic matter and to diagenetic re-precipitation of Fe-oxide (Franke & Paul 1980).

467 This is the case, for example, of condensed pelagic carbonates across the Givetian/Frasnian

468 boundary, where Devleeschouwer et al. (2015) drew attention to the fact that the ferro-

469 magnetic fraction may contain high coercivity minerals such as hematite and goethite of

470 secondary origin that could affect the MS signal. This is probably also the case in the CT

471 section, but no hysteresis analyses are available to confirm the assumption that the observed

472 positive excursions may be solely related to hematization during diagenesis. Post-depositional

473 transformation of paramagnetic clay minerals may also alter the detrital signal of MS.

474 However, this is not the case because the burial temperature was less than 100° (CAI 2-2.5) in

475 CT (Wiederer et al. 2002). It is noteworthy however, that, at CT, the Griotte limestones were

476 deposited on an unstable slope under current activity and underwent repeated intra-

477 formational submarine sliding (debris flows, slumping…) (Girard et al. 2014), leading to local

478 accumulation of Fe-rich sediments. These events may correspond to anomalously high

479 positive peaks in the MS curve at the base of the *Pa*. *marginifera marginifera* Zone (Fig. 2).

480   At the basins scale, the scenario of MS positive excursions coinciding with hematite-

481 rich early Famennian Griotte limestones has to be discussed. The Griottes limestones are

482 commonly found in southern Europe including the Pyrenees, Montagne Noire and Carnic

483 Alps. Nevertheless, they do not exist in contemporaneous strata in Sardinia despite a similar

484 MS signal. Moreover, this facies is not present in the Thuringian Buschteich section where the

485 MS variation pattern is the same. Conversely, at the beginning of the mid-Famennian, high

486 MS values characterize also compact reddish and brown calcilutites with iron-oxide coatings

487 on the shallow northern Tafilalt platform subjected to emergences (Buggisch & Clausen 1972,

488 Wendt & Aigner 1985). It is noteworthy that a different scenario prevails in the Rhenish slate-

489 mountains where condensed carbonate deposits on deep-water submarine rises upon volcanic

490 substrates at Sessacker are red-coloured despite rather low MS values. At BHT similar low

491 values, after a marked positive excursion in the earliest Famennian (Riquier et al. 2010),

492 occur in mud-mound carbonates which are not red-colored (Schülke & Popp 2005).

493 In summary, the MS variations during the Famennian is independant from the presence of red

494 facies (Griottes or others), and are consequently interpreted as primary. Consequently, the

495 effect of post-depositional processes probably did not significantly overprint those of sea level

496 changes during the Famennian to explain the differences between the records of Gondwana

497 and Laurussia, especially the high MS values during the early Famennian in North

498 Gondwana.

499

5.3. Influence of sea-level changes

501 Magnetic susceptibility and conodont biofacies are potentially interrelated: MS could

502 be a proxy to evaluate detrital input if the signal is of primary origin, and conodont biofacies

503 are interpreted as related to water depth due to habitat preferences of the different conodont

504 genera along a proximal-distal gradient in the surface waters. Conodont PC1 displays a strong

505 relationship with magnetic susceptibility in N-Gondwana terranes, and also on Laurussia, at

506 least for Sessacker, and as such suggests constituting a real indicator of sea-level variations

507 during the Famennian: low MS signals indicate a transgressive trend and correspond to distal

508 biofacies, and, inversely, high MS signals indicate a regressive trend and correspond to

509 proximal biofacies.

510 The shift towards lower values for MS and the trend to negative values on the PC1 in

511 N-Gondwana terranes coincides with a local T-R (transgressive - regressive) couplet called

512 "Enkeberg event" described in Laurussia (Rhenish Slate Mountains; House 1985). In

513 Avalonia (Laurussia), there is no major significant change in MS values but the Enkeberg

514 event was identified in the faunal record (Becker 1993). This event has not been yet identified

22

in the North Gondwana terranes. Consequently, the differences in the MS records of N-

516 Gondwana and S-Laurussia rely on other factors, such as paleoclimate and paleogeography.

517

5.4. Paleoclimate and paleo-latitude

519   During the Famennian, SES, BHT, BU, and PZW sections were located in the

520 subtropical zone of the southern hemisphere (Fig. 1). A long-term discrete cooling occurred

521 during the Famennian, but no major changes in temperatures of the sea-surface waters was

522 recorded (Joachimski et al. 2009); this may exclude a major role of physico-chemistry

523 parameters of sea water conditions on MS values. Following the draw-down of atmospheric

524 CO_2 concentrations and burial of organic carbon during the end-Frasnian Kellwasser crises,

525 oxygen isotope values in conodont apatite indicate a global mean temperature drop of low

526 latitude surface-water in post-event early Famennian times (Balter et al. 2008; Joachimski &

527 Buggisch 2002; Joachimski et al. 2009). Mean sea-surface temperatures estimated from

528 conodont apatite $\delta^{18}O$ values in the Rhenish Slate Mountains (Beringhauser Tunnel section)

529 seem to be slightly higher than in Gondwana related terranes (Thuringia, Carnic Alps,

530 Southern France) (Joachimski et al. 2009). Concerning climate, the main difference between

531 Gondwana and Laurussia could rely on the latitudinal position between sites on the

532 subtropical Laurussia and those of North Gondwana that are farther south in a more temperate

533 position. Indeed, emerged parts of North Gondwana would have accentuated seasonality of

534 climate and enhanced continental weathering (Percival et al. 2019; Herman et al. 2013).

535 Therefore, emerged areas within the North Gondwana domain might have provided larger

536 amounts of detrital material than the emerged parts of Laurussia. The decrease of high MS

537 values on the Gondwana shelf began during the *Pa. rhomboidea* highstand of sea level and

538 was probably achieved during the following transgressive pulse of the Enkeberg Event during

539 the early mid-Famennian (Sandberg et al. 2002).

540

5.5. Dynamic paleogeography

Though still debated, Late Devonian plate tectonic models postulate convergence and collisional events between Gondwana and Laurussia heralding both the onset and the development of the Variscan orogeny. Subduction of oceanic crusts between Gondwana-derived continentsled successively to the closure from S to N of several oceanic basins (including, Saxo-Thuringian, Rheno-Hercynian oceans...) that previously separated Armorican terranes (e.g., Thuringia, Bohemia) from the southern Laurussian margin (Franke et al. 2017, Golonka 2020) (Fig. 1). This resulted in the formation of large carbonate platforms on distal marine shelves on the Gondwana margins (parts of NW Africa to Montagne Noire). Opposite, on the southern margin Laurussia (Thuringia microcontinent), condensed pelagic limestones were restricted to tectonic or volcanic submarine highs.

During the early Famennian, only the narrowing oceanic interspaces of the Rheno-hercynian basin, assumed width was 1000 km during the Frasnian, separated Laurussia from outer-shelves of Gondwana-derived terranes (Franke et al. 2017). The age of the closure of the Rheic Ocean remains debated. After Franke (2019) it closed during the Early Devonian times. Other models maintained the Rheic ocean open between Saxo-Thuringia and Avalonia until the Carboniferous (Eckelmann et al. 2014; Golonka 2020, fig. 4). Nevertheless, all these models consider that the northern Gondwana shelf was much more extensive during the Famennian than those of South Laurussia which were restricted to narrow submarine highs and troughs. In such a setting, the detrital supplies from emerged source areas to carbonate platforms were naturally more homogenously dispatched in the N-Gondwana shelf than in the Laurussia margin. Opposite, the accumulation of the detrital material in the Laurussia margin, even if locally important, was in fact located in troughs (e.g., Rhenish area) and low MS values are recorded on the rises. Consequently, the N-Gondwana and South Laurussia

24

565 margins clearly underwent a different paleogeographic behavior, and thus a different setting

566 for detrital accumulation.

567   The separation between the two margins by the narrowing Rheno-Hercynian Ocean is

568 effective at least until the beginning of the mid-Famennian, even if some local pelagic

569 deposits can be found till the early Carboniferous (Franke et al. 2017). From the *Pa.*

570 *marginifera marginifera* Zone onwards to the latest Famennian the effectiveness of the

571 separation apparently vanished when climate became cooler (Girard et al. 2020). MS values

572 considerably dropped and became conform to median values throughout the entire region

573 between the Avalonian margins of Laurussia and N-Gondwana related terranes.

574 Consequently, more uniform conditions and smaller amounts of detrital supply prevailed

575 throughout. Concomitantly, the conjunction of vicinity of the two margins and similar

576 climatic conditions is also corroborated by the increasing identity of stenotopic level-bottom

577 biotas such as phacopid trilobites (Feist 2019) in both areas. Consequently, during this time

578 interval, we condider that mid-late Famennian deposits with low MS values seems to be

579 controlled by first an evolving paleogeographic setting, and, at a lesser extent, eustasy, current

580 activity and climate. This paleogeographic setting results from converging margins prior to

581 closure, and questions the existence, during mid-late Famennian, of wide oceanic domains.

582

583

Conclusions

585   The MS study of five sections in the N-Gondwana margin shows high and oscillating

586 values during the early Famennian, and low values during the mid-late Famennian. In the S-

587 Laurussia margin, MS values remain low through the whole Famennian. Geochemical

588 investigations, and hysteresis parameters in three N-Gondwana sections indicate that the

589 diagenetic processes did not significantly overprint the primary signal of MS. This is

590 emphasized by the degree of burial, thus the temperature during diagenesis (CAI of

591 conodonts) and the presence or absence of red facies, as the MS values remain consistent

592 from one section to other.

593 For the first time, we demonstrate a high correlation between these MS and conodont

594 biofacies, confirming their validity for sea level reconstructions. Taking into account all the

595 above mentioned studies, MS can now be used for paleogeographic reconstructions in the

596 presently dismembered areas of the Variscan Belt.

597 During the early Famennian, the difference in the MS trends and the high values in N-

598 Gondwana compared to S-Laurussia can be explained by two main paleogeographic

599 constraints: i) the Rheic Ocean was not closed; ii) the North-Gondwana margin was wide

600 whilst the South Laurussia margin was fragmented into rises and troughs. During the mid-late

601 Famennian, the uniformization of MS toward low values is interpreted as indicative of rather

602 similar conditions in both margins, linked to plate convergence and vanishing influence of

603 oceanic spaces.

604

605

606

607 **Declaration of competing interest**

608 The authors declare that they have no known competing financial interests or personal

609 relationships that could have appeared to influence the work reported in this paper.

610

26

References

623 Averbuch, O., Tribovillard, N., Devleeschouwer, X., Riquier, L., Mistiaen, B., Van Vliet-
624   Lanoe, B., 2005. Mountain building-enhanced continental weathering and organic carbon
625   burial as major causes for climatic cooling at the Frasnian-Famennian boundary (c. 376
626   Ma)? Terra Nova 17, 25-34.

627 Balter, V., Renaud, S., Girard, C., Joachimski, M.M., 2008. Record of climate-driven
628   morphological changes in 376 Ma Devonian fossils. Geology 36, 907-910.

629 Becker, R.T., 1993. Anoxia, eustatic changes, and upper Devonian to lowermost
630   Carboniferous global ammonoid diversity, In: House, M.R. (Ed.), The Ammonoidea:
631   Environment, Ecology, and Evolutionary Change. Systematics Assoc. Spec. Vol., Oxford,
632   pp. 115-163.

633 Becker, R.T., Gradstein, F.M., Hammer, O., 2012. The Devonian Period, in: Gradstein, F.M.,
634   Ogg, J.G., Schmitz, M.D., Ogg, G.M. (Eds.), The Geologic Time Scale 2012. Elsevier,
635   Oxford, pp. 559-602.

636 Becker, R.T., Marshall, J.E.A., Da Silva, A.-C., 2020. The Devonian Period. In Geological
637   Time Scale 2020. doi: https://doi.org/10.1016/B978-0-12-824360-2.00022-X

638 Buggisch, W., Clausen, C.-D., 1972. Conodonten- und Goniatiten-Faunen aus dem oberen
639   Frasnium und unteren Famennium Marokkos (Tafilalt, Antiatlas). Neues Jahrb. Geol.
640   Palaontol. Abh. 141, 137-167.

641 Clarkson, M.O., Poulton, S.W., Guilbaud, R., Wood, R.A., 2014. Assessing the utility of
642   Fe/Al and Fe-speciation to record water column redox conditions in carbonate-rich
643   sediments. Chem. Geol. 382, 111-122.

644 Corradini, C., 1998. Famennian conodonts from two sections near Villasalto. Giorn. Geol. 60,
645   Spec. Issue, 122-135.

646 Corradini, C., 2003. Late Devonian (Famennian) conodonts from the Corona Mizziu Sections
647   near Villasalto (Sardinia, Italy). Palaeontogr. Ital. 89, 65-116.

648 Corradini C., Mossoni A., Corriga M.G., Spalletta C., 2021. The Devonian/Carboniferous
649   Boundary in Sardinia (Italy). Paleobiodivers. Paleoenviron. 101. doi: 10.1007/s12549-
650   019-00411-5

651 Corradini, C., Mossoni, A., Pondrelli, M., Simonetto, L., 2017. Famennian conodonts in the
652   Mt. Pizzul West (PZW) section. Ber. Inst. Erdwiss. K.F.-Univ. Graz, 23, 246-250.

Crick, R.E., Ellwood, B.B., Feist, R., El Hassani, A., Schindler, E. Dreesen, R. Over, D.J., Girard, C., 2002. Magnetostratigraphy susceptibility of the Frasnian/Famennian boundary. Palaeogeogr. Palaeoclimatol. Palaeoecol. 181, 67-90.

Da Silva A.C., Mabille C., Boulvain F., 2009. Influence of sedimentary setting on the use of magnetic susceptibility: examples from the Devonian of Belgium. Sedimentology 56, 1292-1306.

Da Silva A.C., Yans J., Boulvain F., 2010. Sedimentology and magnetic susceptibility during the "punctata" event of the Ardenne area (Belgium): identification of severe and rapid sea level fluctuations. In: Da Silva, AC. and Boulvain, F. (eds): magnetic susceptibility, correlations and Palaeozoic environments. Geol. Belg. 13/4, 319-332.

Da Silva, A.-C., Whalen, M.T., Hladil, J., Chadimova, L., Chen, D., Spassov, S., Boulvain, F., Devleeschouwer, X., 2015. Magnetic susceptibility application: a window onto ancient environments and climatic variations: foreword. Geol. Soc. Spec. Publ., London 414, 1-13.

Da Silva, A.C., Dekkers, M.J., Mabille, C., Boulvain, F., 2012. Magnetic signal and its relationship with paleoenvironments and diagenesis - examples from the Devonian carbonates of Belgium. Studia Geophys. Geod. 56, 677-704.

Davies, E.J., Ratcliffe, K.T., Montgomery, P., Pomar, L., Ellwood, B.B., Wray, D.S., 2013. Magnetic Susceptibility (χ) Stratigraphy and Chemostratigraphy Applied to an Isolated Carbonate Platform Reef Complex; Llucmajor Platform, Mallorca, In: Verwer, K., Playton, T.E., Harris, P.M.M. (Eds.), Deposits, Architecture, and Controls

Devleeschouwer, X., Petitclerc, E., Spassov, S., Préat, A., 2010. The Givetian-Frasnian boundary at Nismes parastratotype (Belgium): the magnetic susceptibility signal controlled by ferromagnetic minerals. Geol. Belg., 14/4, 345-360.

Devleeschouwer, X., Riquier, L., Bábek, O., Devleeschouwer, D., Petitclerc, E., Sterckx, S., Spassov, S., 2015. Magnetization carriers of gry to red deep-water limestones in the GSSP of the Givetian-Frasnien boundary (Puech de la Suque, France): signals influenced by moderate diagenetic overprinting, In: Da Silva, A.C., Whalen, M.T., Hladil, J., Chadimova, L., Chen, D., Spassov, S., Boulvain, F., Devleeschouwer, X. (Eds.), Magnetic Susceptibility Applications: A Window onto Ancient Environments and Climatic Variations. Geol. Soc. Spec. Publ., London 414 (1), 157-180.

Eckelmann, K., Nesbor, H.-D., Königshof, P., Linnemann, U., Hofmann, M., Lange, J.-M., Sagawe, A., 2014. Plate interactions of Laurussia and Gondwana during the formation of Pangaea — Constraints from U–Pb LA–SF–ICP–MS detrital zircon ages of Devonian and Early Carboniferous siliciclastics of the Rhenohercynian zone, Central European Variscides. Gondwana Res. 25, 1484-1500.

Ellwood B.B., Garcia-Alcalde J.L., El Hassani A., Hladil J., Soto, F.M., Truyols-Massoni, M., Weddige, K., Koptikova, L., 2006. Stratigraphy of the Middle Devonian Boundary: Formal Definition of the Susceptibility Magnetostratotype in Germany with comparisons to Sections in the Czech Republic, Morocco and Spain. Tectonophysics 418, 31-49.

Ellwood B.B., Tomkin J., Richards B., Benoist S.L., Lambert L.L., 2007. MSEC Data Sets Record Glacially Driven Cyclicity: Examples from the Arrow Canyon Mississippian-Pennsylvanian GSSP and Associated Sections. Palaeogeogr. Palaeoclimatol. Palaeoecol. 255, 377-390. doi: 10.1016/j.palaeo.2007.08.006.

697 Ellwood B.B., Tomkin J.H., Ratcliffe K.T., Wright M., Kafafy A.M., 2008. High-resolution
698   magnetic susceptibility and geochemistry for the Cenomanian/Turonian boundary GSSP
699   with correlation to time equivalent core. Palaeogeogr. Palaeoclimatol. Palaeoecol. 261,
700   105-126.

701 Ellwood, B.B., Algeo, T., El Hassani, A., Tomkin, J.H., Rowe, H., 2011a. Defining the
702   Timing and Duration of the Kačák Interval within the Eifelian/Givetian Boundary GSSP,
703   Mech Irdane, Morocco, Using Geochemical and Magnetic Susceptibility Patterns.
704   Palaeogeogr. Palaeoclimatol. Palaeoecol. 304, 74–84.

705 Ellwood, B.B., Balsam, W.L., Roberts, H.H., 2006. Gulf of Mexico Sediment Sources and
706   Sediment Transport Trends from Magnetic Susceptibility Measurements of Surface
707   Samples. Mar. Geol. 230, 237–248.

708 Ellwood, B.B., Tomkin, J.H., El Hassani, A., Bultynck, P., Brett, C.E., Schindler, E., Feist,
709   R., Bartholomew, A.J., 2011b. A climate-driven model and development of a floating point
710   time scale for the entire Middle Devonian Givetian Stage: A test using
711   magnetostratigraphy susceptibility as a climate proxy. Palaeogeogr. Palaeoclimatol.
712   Palaeoecol. 304, 85-95.

713 Epstein, A., Epstein, J., Harris, L. 1977. Conodont Color Alteration - an Index to Organic
714   Metamorphism. Geol. Surv. Prof. Pap. 995, 1-27. doi:10.3133/pp995.

715 Feist, R., 2019. Post-Kellwasser event recovery and diversification of phacopid trilobites in
716   the early Famennian (Late Devonian). Bull. Geosci. 94, 1-22.

717 Franke, W. Walliser, O.H. 1983. "Pelagic" carbonates in the Variscan Belt – their
718   sedimentary and tectonic environments, In: Martin H. and Eder F. W., Intercontinental
719   Fold Belts. Springer, Berlin, pp. 77-92.

720 Franke, W., Cocks, L.R.M., Torsvik, T.H., 2017. The Palaeozoic Variscan oceans revisited.
721   Gondwana Res. 48, 257-284.

722 Franke, W., Cocks, L.R.M., Torsvik, T.H., 2019. Detrital zircons and the interpretation of
723   palaeogeography, with the Variscan Orogeny as an example. Geol. Mag. 157 (4), 1-5.
724   doi.org/10.1017/S0016756819000943

725 Franke, W., Paul, J. 1980. Pelagic redbeds in the Devonian of Germany – deposition and
726   diagenesis. Sediment. Geol. 25, 231-256.

727 Girard, C., Cornée, J.-J., Charruault, A.-L., Corradini, C., Weyer, D., Bartzsch, K.,
728   Joachimski, M.M., Feist, R., 2017. Conodont biostratigraphy and palaeoenvironmental
729   trends during the Famennian (Late Devonian) in the Thuringian Buschteich section
730   (Germany). Newsl. Stratigr. 50, 71-89.

731 Girard, C., Cornée, J.-J., Corradini, C., Fravalo, A., Feist, R., 2014. Palaeoenvironmental
732   changes at Col des Tribes (Montagne Noire, France), a reference section for the Famennian
733   of north Gondwana-related areas. Geol. Mag. 151, 864-884.

734 Girard, C., Cornée, J.-J., Joachimski, M.M., Charruault, A.-L., Dufour, A.-B., Renaud, S.,
735   2020. Paleogeographic differences in temperature, water depth and conodont biofacies
736   during the Late Devonian. Palaeogeogr. Palaeoclimatol. Palaeoecol. 549, 108852.
737   https://doi.org/10.1016/j.palaeo.2018.06.046

738 Golonka, J., 2020. Late Devonian paleogeography in the framework of global tectonics.
739   Global Planet. Change 186. https://doi.org/10.1016/j.gloplacha.2020.103129

Herman, F., Seward, D., Valla, P.G., Carter, A., Kohn, B., Willett, S.D., Ehlers, T.A., 2013. Worldwide acceleration of mountain erosion under a cooling climate. Nature 504.

Hladil, J., 2002. Geophysical records of dispersed weathering products on the Frasnian carbonate platform and early Famennian ramps in Moravia, Czech Republic: proxies for eustasy and palaeoclimate. Palaeogeogr. Palaeoclimatol. Palaeoecol. 181, 213-250.

House, M.R., 1985. Correlation of mid-Palaeozoic ammonoid evolutionary events with global sedimentary perturbations. Nature 313, 17-22.

Joachimski, M., Buggisch, W., 2002. Conodont apatite $\delta^{18}O$ signatures indicate climatic cooling as a trigger of the Late Devonian mass extinction. Geology 30, 711-714.

Joachimski, M.M., Breisig, S., Buggisch, W., Talent, J.A., Mawson, R., Gereke, M., Morrow, J.R., Day, J., Weddige, K., 2009. Devonian climate and reef evolution: Insights from oxygen isotopes in apatite. Earth Planet. Sci. Lett. 284, 599-609.

Johnson, J.G., Klapper, G., Elrick, M., 1996. Devonian transgressive-regressive cycles and biostratigraphy, Northern Antelope Range, Nevada: establishment of reference horizons for global cycles. Palaios 11, 3-14.

Johnson, J.G., Klapper, G., Sandberg, C.A., 1985. Devonian tatic fluctuations in Euramerica. Geol. Soc. Am. Bull. 96, 567-587.

Klapper, G., Barrick, J.E., 1978. Conodont ecology: pelagic versus benthic. Lethaia 11, 15-23.

Mossoni, A., 2014. Selected Famennian (Late Devonian) events (Condroz, Annulata, Hangenberg) in Sardinia and in the Carnic Alps: conodont biostratigraphy, magnetic susceptibility and geochemistry, Università degli Studi di Cagliari. Cagliari, p. 171 (unpublished thesis).

Over, D.J., Hauf, E., Wallace, J., Chiarello, J., Over, J.-S., Gilleaudeau, G.J., Song, Y., Algeo, T.J., 2019. Conodont biostratigraphy and magnetic susceptibility of Upper Devonian Chattanooga Shale, eastern United States: Evidence for episodic deposition and disconformities. Palaeogeogr. Palaeoclimatol. Palaeoecol. 524, 137-149. https://doi.org/10.1016/j.palaeo.2019.03.017.

Percival, L.M.E., Selby, D., Bond, D.P.G., Rakociński, M., Racki, G., Marynowski, L., Adatte, T., Spangenberg, J.E., Föllmi, K.B., 2019. Pulses of enhanced continental weathering associated with multiple Late Devonian climate perturbations: Evidence from osmium-isotope compositions. Palaeogeogr. Palaeoclimatol. Palaeoecol. 524, 240-249.

Riquier, L., Averbuch, O., Devleeschouwer, X., Tribovillard, N., 2010. Diagenetic versus detrital origin of the magnetic susceptibility variations in some carbonate Frasnian-Famennian boundary sections from Northern Africa and Western Europe: implications for paleoenvironmental reconstructions. Int. J. Earth Sci. 99, 57-73.

Sandberg, C.A., 1976. Conodont biofacies of late Devonian *Polygnathus styriacus* Zone in western United States, In: Barnes, C.R. (Ed.), Conodont Paleoecology. Geol. Assoc. Canada spec. Pap. Montreal, pp. 171-186.

Sandberg, C.A., Morrow, J.R., Ziegler, W., 2002. Late Devonian sea-level changes, catastrophic events, and mass extinctions. Geol. Soc. Am. Spec. Pap. 356, 473-487.

Schülke, I., 1995. Evolutive Prozesse bei *Palmatolepis* in der frühen Famenne-Stufe (Conodonta, Ober-Devon). Göttinger Arbeiten zur Geologie und Pälaontologie, Göttingen.

783 Schülke, I., 1999. Conodont multielement reconstructions from the the early Famennian (Late
784   Devonian) of the Montagne Noire (southern France). Geol. Palaeontol. 31, 1-123.

785 Schülke, I., Popp, A., 2005. Microfacies development, sea-level change, and conodont
786   stratigraphy of Famennian mid- to deep platform deposits of the Beringhauser Tunnel
787   section (Rheinisches Schiefergebirge, Germany). Facies 50, 647-664.

788 Seddon, G., Sweet, W.C., 1971. An ecologic model for conodonts. J. Paleontol. 45, 869-880.

789 Spalletta, C., Perri, M.C., Over, D.J., Corradini, C. 2017. Famennian (Upper Devonian)
790   conodont zonation: revised global standard. Bull. Geosci. 92 (1), 31-57.

791 Tucker, E., 1974. Sedimentology of Palaeozoic pelagic limestones: the Devonian Griotte
792   (Southern France) and Cephalopodenkalk (Germany). Spec. Pub., Intern. Assoc.
793   Sedimentologists 1, 71-92.

794 Wendt, J., Aigner, T., 1985. Facies patterns and depositional environments of Palaeozoic
795   cephalopod limestones. Sediment. Geol. 44, 263-300. http://doi.org/10.1144/SP414.15

796 Wiederer, U., Königshof, P., Feist, R., Franke, W. and Doublier M. P. 2002. Low-grade
797   metamorphism in the Montagne Noire (S-France): Conodont Alteration Index (CAI) in
798   Palaeozoic carbonates and implications fort he exhumation of a hot metamorphic core
799   complex. Schweiz. mineral. petrogr. Mitt. 82, 393-407.

800 Ziegler, W., 1962. Taxionomy und Phylogenie oberdevonischer Conodonten und ihre
801   stratigraphische Bedeutung. Abh. hess. Landesamt. Bodenforsch. Wiesbaden.

802

803

Figure captions

805 **Figure 1**. **a)** Early Famennian (-370.3 Ma) paleogeographic map (after Franke et al., 2017 and

806 Golonka, 2020) showing the locations of the studied sections.

807 Abbreviations: SES: Sessacker (Rhenish Slate Mountains, Germany), BHT: Beringhauser

808 Tunnel (Rhenish Slate Mountains, Germany), PZW: Pizzul West (Carnic Alps, Italy), CT:

809 Col des Tribes (Montagne Noire, France), CM: Corona Mizziu (Sardinia, Italy), BU:

810 Buschteich (Thuringia, Germany), ERF: Erfoud (Tafilalt, SE Morocco), DGHS (DuPont GHS

811 Core, Eastern United States, after Over et al. 2019). **b)** Biostratigraphic correlation of the the

812 studied sections.

813

814 **Figure 2**. Magnetic susceptibility curves through the Famennian (Late Devonian) for sections

815 of S-Laurussia and N-Gondwana. Ages based on Girard et al. (2020), and updated after

816 Becker et al. (2020). The curves represent the average of the MS values obtained with 2 to 5

817 measurements with the standard error in grey. Vertical dotted line: average MS values for

818 lithified marine deposits estimated to 5. 5 x 10^{-8} m3/kg (Ellwood et al. 2011a). Data of DGHS

819 (Eastern United States) are after Over et al. (2019) and data of uppermost Frasnian to lower

820 Famennian in Coumiac (CUQ*) and Berinhauser Tunnel (BHT*) after Riquier et al. (2010).

821 Conodont Zones after Spalletta et al. (2017).

822

823 **Figure 3**. **a)** Magnetic susceptibility curves through the Famennien (Late Devonian) at Col

824 des Tribes (CT, France) in green, Buschteich (BU, Germany) in red and Corona Mizziu (CMI

825 and CM II, Italia) in orange, Sessacker (SES) in black. **b)** Conodont biofacies through time

826 depicted as variations along the first axis of the PCA on conodont genera percentages of CT

827 (in green), BU (in red), CM (dotted line in orange), and (SES) in black. **c)** Simplified

828 transgressive-regressive cycles after Johnson et al. (1985, 1996). Conodont Zones after

829 Spalletta et al. (2017). Ages based on Girard et al. (2020), modified after Becker et al. (2020).

830

831

832 **Supplementary Figure 1**. Low field magnetic susceptibility (χLF) and geochemical data

833 (Al_2O_3, SiO_2, Fe_2O_3, TiO_2, K_2O) for the PZW, CM II and CM I sections.

834

835 **Supplementary Figure 2.** Scatterplots reporting the MS versus selected geochemical indexes

836 for samples from the Buschteich section (Level BU03 not figured). **a)** The zirconium (Zr)

837 concentration (ppm); **b)** the iron (Fe) concentration (%); **c)** Fe_{exc} (%), **d)** Fe_{det} (%). The

838 number of samples, the correlation coefficient r, and the p are reported for each diagram.

839 Open red circles: levels after the "Enkeberg event", Red coloured circles: levels before the

840 "Enkeberg event".

841

842 **Supplementary Table 1**. Magnetic susceptibility (MS) for the Col des Tribes (CT) section.

843 MS in m^3/kg. Depth in cm. Conodont Zones after Spalletta et al. (2017). Ages based on

844 Girard et al. (2020), and modified after Becker et al. (2020).

845

846 **Supplementary Table 2**. Magnetic susceptibility (MS) for the Buschteich (BU) section. MS

847 in m^3/kg. Depth in cm. Conodont Zones after Spalletta et al. (2017). Ages based on Girard et

848 al. (2020), and modified after Becker et al. (2020). Concentrations in Fe, Al, Zr (in ppm), and

849 associated errors.

850

851 **Supplementary Table 3**. Magnetic susceptibility (MS) for the Sessacker (SES) section. MS

852 in m^3/kg. Depth in cm. Conodont Zones after Spalletta et al. (2017). Ages based on Girard et

853 al. (2020), and modified after Becker et al. (2020).

854

855 **Supplementary Table 4**. Magnetic susceptibility (MS) for the Beringhauser Tunnel (BHT)

856 section. MS in m^3/kg. Depth in cm. Conodont Zones after Spalletta et al. (2017). Ages based

857 on Girard et al. (2020), and modified after Becker et al. (2020).

858

859   **Supplementary Table 5**. Magnetic susceptibility (MS) for the Erfoud (ERF) section. MS in

860   m^3/kg. Depth in cm. Conodont Zones after Spalletta et al. (2017). Ages based on Girard et al.

861   (2020), and modified after Becker et al. (2020).

862

863   **Supplementary Table 6**. Magnetic susceptibility (MS) for the Pizzul West (PZW) section.

864   MS in m^3/kg. Depth in cm. Conodont Zones after Spalletta et al. (2017). Ages based on

865   Girard et al. (2020), and modified after Becker et al. (2020).

866

867   **Supplementary Table 7**. Magnetic susceptibility (MS) for the Corona Mizziu II (CM II)

868   section. MS in m^3/kg. Depth in cm. Conodont Zones after Spalletta et al. (2017). Ages based

869   on Girard et al. (2020), and modified after Becker et al. (2020).

870

871   **Supplementary Table 8**. Magnetic susceptibility (MS) and low field magnetic susceptibility

872   (χLF), ferromagnetic contribution (χFerro), hysteresis parameters (high field magnetic

873   susceptibility (χHF)), saturation magnetization (MS), coercitive force (Hc), coercivity of

874   remanence (Hcr), highfield remanence and viscosity decay; geochemical data for Corona

875   Mizziu I (CM I) section.

876

877   **Supplementary Table 9.** Low field magnetic susceptibility (χLF), ferromagnetic contribution

878   (χFerro), hysteresis parameters (high field magnetic susceptibility (χHF)), saturation

879   magnetization (MS), coercitive force (Hc), coercivity of remanence (Hcr), highfield

880   remanence and viscosity decay, geochemical data for the Corona Mizziu II (CM II) section.

881

882   **Supplementary Table 10.** Low field magnetic susceptibility (χLF), ferromagnetic

883   contribution (χFerro), hysteresis parameters (high field magnetic susceptibility (χHF)),

884   saturation magnetization (MS), coercitive force (Hc), coercivity of remanence (Hcr), highfield

885   remanence and viscosity decay and geochemical data for the Pizzul West (PZW) section.

886

887   **Supplementary Table 11.** Mean MS (m^3/kg), and conodont genera percentages (pc). Names

888   of the samples: CT (Col des Tribes), BU (Buschteich), SES (Sessacker), CM (Corona

889   Mizziu). Ages are given by the conodont zones after Spalletta et al. (2017) and by the age

890   model (in My). Proportions of the different genera: pcPa: *Palmatolepis*; pcPo: *Polygnathus*;

891   pcAn: *Ancyrognathus* and *Ancyrodella*; pcIc: *Icriodus*; pcBi: *Bispathodus*, *Branmehla* and

892   *Mehlina*; pcSc. *Scaphignathus* and *Alternognathus*, pcSi: *Siphonodella*.

Table 1. Correlations between MS (χLF), and ferromagnetic contribution (χFerro), high field magnetic susceptibility (χHF), coercivity of remanence (Hcr), and geochemical data using linear regression. Number of samples (N), coefficient of correlation (r) and probability (p) are given. Significant correlations marked in bold (p < 0.05).

		CM I			CM II			PZW		
		N	r	p	N	r	p	N	r	p
Xlf	Xferro	32	**0.69**	**0.000**	14	**0.85**	**0.000**	20	**0.87**	**0.000**
	Xhf	32	**0.82**	**0.000**	14	**0.82**	**0.000**	21	0.03	0.454
	Hcr	32	**0.68**	**0.000**	14	0.74	**0.002**	21	0.03	0.422
Xlf	Al2O3	13	0.68	**0.010**	11	0.25	0.463	17	0.005	0.785
Xhf		13	0.48	0.095	11	0.27	0.915	17	**0.84**	**0.000**
Xlf	SiO2	13	0.51	0.072	11	0.47	0.146	17	0.12	0.653
Xhf		13	0.55	0.050	11	0.49	0.122	17	**0.81**	**0.000**
Xlf	Fe2O3	13	0.70	**0.008**	11	0.67	**0.023**	17	0.13	0.613
Xhf		13	0.50	0.081	11	0.39	0.239	17	**0.92**	**0.000**
Xlf	TiO2	13	0.70	**0.008**	11	0.30	0.361	17	0.12	0.655
Xhf		13	0.48	0.096	11	0.31	0.350	17	**0.85**	**0.000**
Xlf	K2O	13	0.70	**0.008**	11	0.08	0.805	17	0.04	0.890
Xhf		13	0.45	0.123	11	0.46	0.158	17	**0.83**	**0.000**
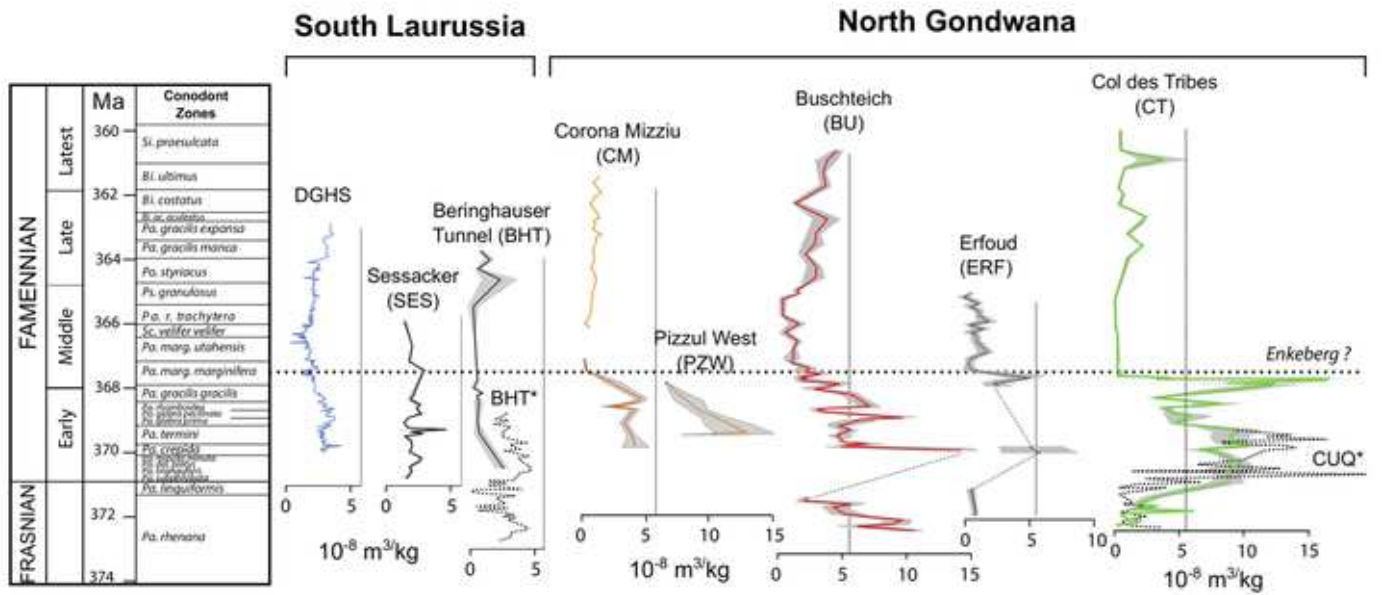
Figure1

Girard et al., Fig. 1

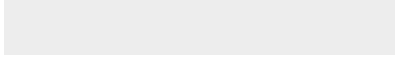Figure 2

Figure3

Figure S1
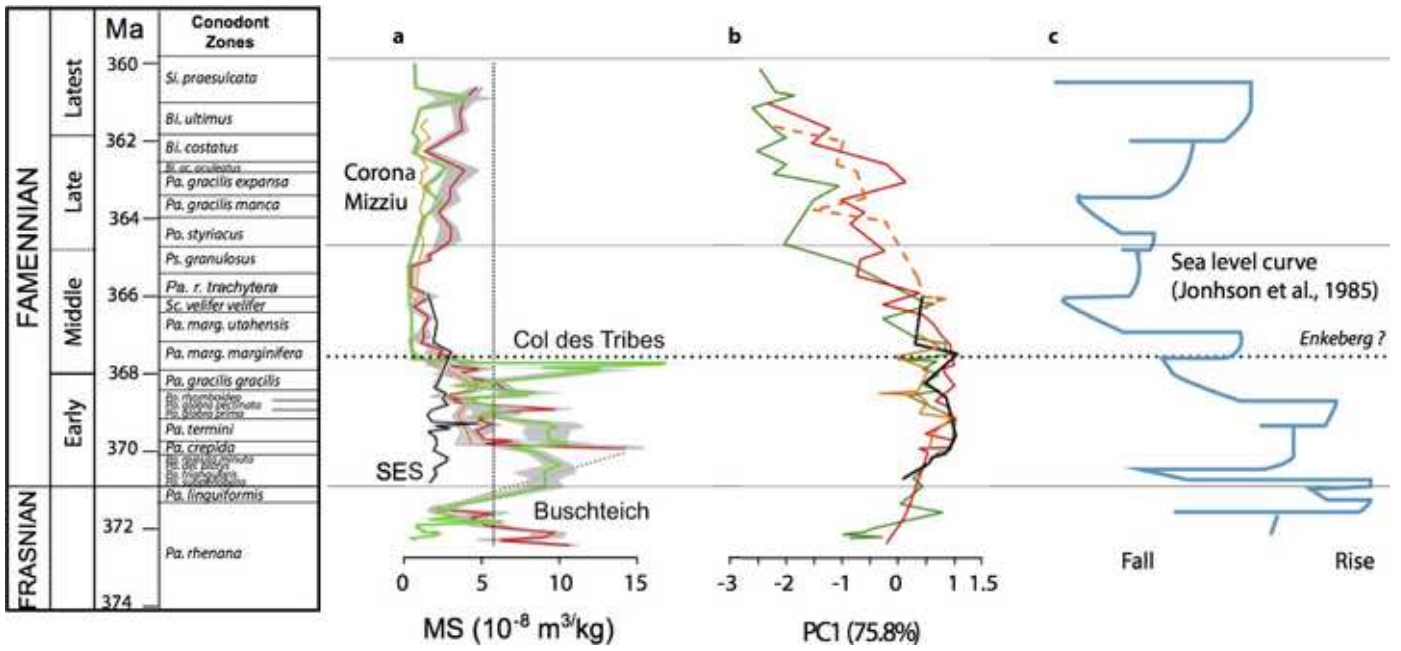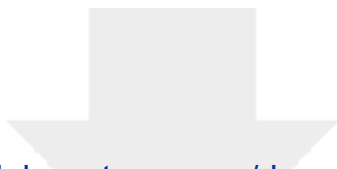
Click here to access/download
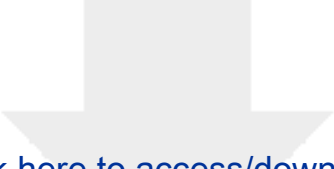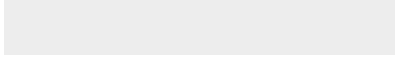**e-component**
Suppl_Fig1_R#2_corrige_apercu.jpg

Figure S2
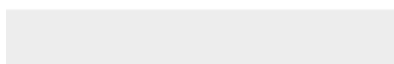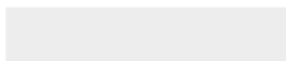
Click here to access/download
e-component
Suppl_Fig2_#1_corrige.jpg

TableS1

TableS2
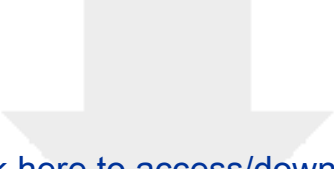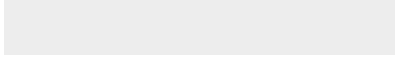
Click here to access/download
e-component
TableS2.docx
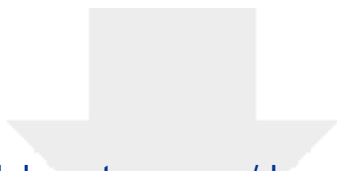
TableS3

Click here to access/download
e-component
TableS3.docx

TableS4

TableS5

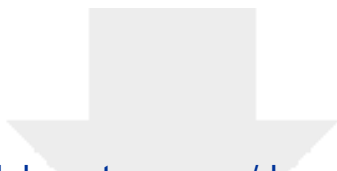Click here to access/download
e-component
TableS5.docx

TableS6

TableS7

Supplementary Table 8

Click here to access/download
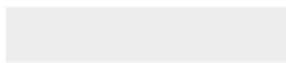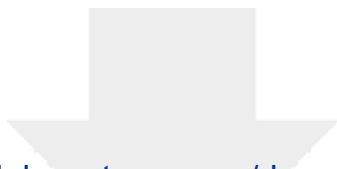**e-component**
Suppl_Table8_CMI_geoch#1.xlsx

Supplementary Table 9
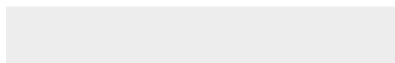
Click here to access/download
e-component
Suppl_Table9_CMII_mean_geoch#1.xls

Supplementary Table 10
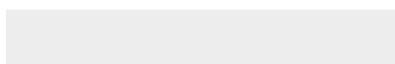
Click here to access/download
e-component
Suppl_Table10_PZW_meangeoch#1bis.xlsx

TableS11

Click here to access/download
e-component
TableS11.docx